



# Studies on the formation and properties of polypyrrole doped with ionised $\beta$ -cyclodextrins: influence of the anionic pendants

Valeria Annibaldi<sup>1</sup> · Gillian M. Hendy<sup>1</sup> · Carmel B. Breslin<sup>1</sup>

Received: 10 October 2018 / Revised: 30 November 2018 / Accepted: 1 December 2018 / Published online: 12 December 2018  
© Springer-Verlag GmbH Germany, part of Springer Nature 2018

## Abstract

Polypyrrole films doped with sulfonated  $\beta$ -cyclodextrin (PPy/s $\beta$ -CD) and carboxymethyl  $\beta$ -cyclodextrin (PPy/CM $\beta$ -CD) were formed on electropolymerisation of pyrrole in a solution of the cyclodextrin sodium salts. Lower rates of electropolymerisation were evident with the carboxymethyl  $\beta$ -CD and this was attributed to protonation of the carboxylate groups due to an increase in the interfacial pH at the electrode–solution interface. The PPy/s $\beta$ -CD and PPy/CM $\beta$ -CD films showed cation exchange behaviour with the ingress of Na<sup>+</sup> and its associated water molecules on reduction. The PPy/CM $\beta$ -CD film showed less electroactive behaviour which may be related to the lower number of anionic pendants on the CM $\beta$ -CD or to the possible precipitation of the less soluble neutral CD which arises due to the protonation of the carboxylate groups. The PPy/s $\beta$ -CD showed a high capacitance of 6.0 mF cm<sup>-2</sup> corresponding to a specific capacitance of 71 F g<sup>-1</sup> over a wide potential range extending from -0.60 to 0.60 V vs SCE. Over-oxidation was observed at relatively low potentials, at about 0.60 V vs SCE. A diffusion coefficient of  $6.47 \times 10^{-6}$  cm<sup>2</sup> s<sup>-1</sup> and a rate constant of  $3.73 \times 10^{-2}$  cm s<sup>-1</sup> were obtained for the ferricyanide redox couple at the PPy/s $\beta$ -CD, indicating little or no inhibition of the ferricyanide redox reaction.

**Keywords** Polypyrrole · Sulfonated  $\beta$ -cyclodextrin · Carboxymethyl  $\beta$ -cyclodextrins · Cation exchange

## Introduction

Polypyrrole is one of the most studied conducting polymer systems, and this is largely due to its ease of preparation and its wide range of applications, that extend from biological sensors to energy storage devices [1, 2]. It is readily formed in the presence of anions that serve to balance the charge on the polypyrrole backbone as the polymer is deposited. These anions are retained in the oxidised polymer film as dopants. The size and charge of the anions influence the properties of the polypyrrole films, with small anions giving the polymer anion-exchange properties, while large immobile anions result in cation exchange [3, 4]. The incorporation of macrocyclic molecules within polypyrrole, such as cyclodextrins or calixarenes, gives the polypyrrole additional recognition sites that can be exploited in a wide range of applications. Several reports have been published on the incorporation of  $\beta$ -

cyclodextrin within the polypyrrole matrix [5–14]. Cyclodextrins are attractive as they are well known to form inclusion complexes with a variety of molecules. Provided the molecule has a suitable size and hydrophobicity, it can form an inclusion complex with the cyclodextrin. It has also been reported that a 1:1 host–guest complex occurs between pyrrole and  $\beta$ -cyclodextrin [11]. The formation of this complex was used to generate hexagonal-shaped polypyrrole particles [12], while polypyrrole nano- and micro-spheres [13] and nano-wires [5] were synthesised using  $\beta$ -cyclodextrin as a molecular template. In addition, cyclodextrins have been employed to electropolymerise bithiophene in aqueous solutions [15]. In this case, the inclusion complex that is formed between bithiophene and the cyclodextrin increases sufficiently the solubility of the monomer, enabling electropolymerisation. Similarly, it has been shown that the solubility of 3,4-ethylenedioxythiophene can be increased in aqueous solutions on forming an inclusion complex, again facilitating the electropolymerisation of the monomer [11].

While the cyclodextrin has an influence during the formation of these polymer systems, it is not clear if the cyclodextrin remains within the final polypyrrole film. However, if the cyclodextrin is used as an anionic dopant, then it will remain

✉ Carmel B. Breslin  
Carmel.Breslin@mu.ie

<sup>1</sup> Department of Chemistry, Maynooth University, Maynooth, County Kildare, Ireland

within the polymer matrix. Indeed, it is possible to use the  $\beta$ -cyclodextrin as a dopant by employing an anionic cyclodextrin, where the rim of the cavity is functionalised with anionic pendants. A number of studies has investigated polypyrrole doped with sulfonated (sulfated)  $\beta$ -cyclodextrin [16–21], with potential applications in the delivery of a neutral drug [17], as sensors [19–21] and in the uptake of cations [18]. These sensing studies suggest that the cavity of the cyclodextrin is sufficiently opened within the polymer matrix and that the cyclodextrin still maintains its recognition properties [19–21]. The studies on the cation uptake are consistent with the large size of the anionic dopant, making it an immobile dopant that is not lost on reduction [18]. Clearly, these cyclodextrin-doped polypyrrole films have a number of potential applications that arise from combining the conducting polymer matrix with an ionisable cyclodextrin that exhibits supramolecular complexing abilities. The incorporation of ionisable cyclodextrins within polypyrrole ensures the dispersion of these charged species, preventing the formation of aggregates and facilitating the formation of host–guest complexes. While various studies have focussed on the formation of polypyrrole in the presence of neutral cyclodextrins, polypyrrole films doped with charged or ionisable cyclodextrins are poorly characterised.

The purpose of this study was to investigate the formation of polypyrrole doped with two anionic cyclodextrins that differ in terms of the anionic pendants. The pendants selected were sulfonated ( $\text{SO}_3^-$ ) and carboxylated ( $\text{COO}^-$ ) groups, which differ in their  $\text{pK}_a$  values. As detailed, sulfonated  $\beta$ -cyclodextrin doped polypyrrole, PPy/s $\beta$ -CD, has been formed previously; however, the applications of the polymer film are the focus in most of these reports and very few details are provided on the formation of the film or on the electropolymerisation of pyrrole in the presence of the large ionisable CD. Tamsamani et al. [16] have described the formation of polypyrrole doped with s $\beta$ -CD; however, a supporting 0.1 M  $\text{LiClO}_4$  electrolyte was employed as the electropolymerisation solution, giving rise to competitive doping. Furthermore, very high potentials of 1.8 V vs SCE were used in the formation of the polymer and this will influence the properties of the final polymer film.

## Experimental

Pyrrole was distilled under vacuum before use and kept refrigerated in the dark to prevent oxidation. Carboxymethyl  $\beta$ -cyclodextrin (CM $\beta$ -CD), with an average of 3.5 anionic carboxylate groups, and sulfonated  $\beta$ -cyclodextrin (s $\beta$ -CD), with a degree of substitution from 7 to 11 mol of sulfonate per mol of  $\beta$ -CD, were obtained from Aldrich as sodium salts. The s $\beta$ -CD was purified further by dissolving the sample in deionised water and then dried under vacuum at a pressure of

0.01 mbar while stirring and heating at 70 °C for 12 h using a Schlenk line. All other chemicals were of analytical reagent grade and used without further purification. Deionised, Milli-Q, water was used for the preparation of all solutions and the pH was maintained at a value of 5.0.

Electrochemical experiments, including potentiostatic, cyclic voltammetry and electrochemical quartz crystal microbalance measurements (EQCM) were carried out using a CHI440 potentiostat (Model EA160), while rotating disc voltammetry experiments were performed using an EG&G, Model 636 ring disc electrode system. A standard three-electrode cell consisting of a working electrode, a Pt wire ( $d = 0.10$  cm) counter electrode and a saturated calomel reference electrode (SCE) was used. The working electrode consisted of glassy carbon ( $d = 4.0$  mm) enclosed in a larger insulating Teflon sheath and set in place using non-conducting epoxy resin. The electrical contact was achieved using a copper wire. The electrodes were polished using 1.0  $\mu\text{m}$  diamond polish (Buehler MetaDi Monocrystalline Diamond suspension) on a Buehler micro-cloth washed with deionised water and sonicated, to ensure a clean and smooth surface. For the EQCM experiments, a silver/silver chloride ( $\text{Ag}|\text{AgCl}$ ) electrode was used as the reference. A gold quartz crystal electrode ( $A = 0.20$   $\text{cm}^2$ ) obtained from IJ Cambria Scientific was used as the working electrode, while a Pt wire ( $d = 0.05$  cm) was employed as the counter electrode. The mass change was computed by monitoring the changes in the frequency of the oscillating quartz crystal. The frequency is related to the mass through the well-known Sauerbrey equation [22], Eq. 1, where  $f_0$  is the resonant frequency,  $\Delta m$  is the mass change,  $A$  is the surface area of the electrode,  $\rho_q$  is the density and  $\mu_q$  is the shear modulus of quartz [22, 23].

$$\Delta f = -\frac{2 f_0^2 \Delta m}{A (\rho_q \mu_q)^{1/2}} \quad (1)$$

Differential scanning calorimetry (DSC) was employed to study the water content of the polymers. A 2.0 mg sample was heated from 30 to 300 °C, at a constant rate of 10 °C  $\text{min}^{-1}$ , under a nitrogen atmosphere. A Perkin Elmer Pyris 6.0 system was used and the data were analysed by means of Pyris Data Analysis software. NMR measurements were carried out by dissolving pyrrole and/or s $\beta$ -CD (a six-fold higher concentration) in  $\text{D}_2\text{O}$  and 0.1 M NaCl. The NaCl was employed to maintain a near constant ionic strength. The data were collected using a 500 MHz NMR spectrometer. The surface morphology of the polymer samples was obtained using a Hitachi scanning electron microscope. The samples were sputter coated with gold using an Emitech K550x gold sputter coater prior to analysis.

The PPy/s $\beta$ -CD was formed using cyclic voltammetry at 0.70 V vs SCE with 0.2 M pyrrole in 0.01 M or 0.02 M s $\beta$ -CD, while the PPy/CM $\beta$ -CD was formed at 0.80 V vs SCE using 0.3 M pyrrole and 0.02 M CM $\beta$ -CD. Unless otherwise stated, the bulk polymers were deposited to a charge density of 0.20 C cm<sup>-2</sup> (equivalent to a charge of 0.025 C). Thinner polymer films were employed for the EQCM analysis, deposited to 0.10 C cm<sup>-2</sup>. No supporting electrolyte was added to the electropolymerisation solutions. For comparative purposes, chloride was used as a dopant and PPy/Cl was formed at 0.70 V vs SCE in 0.2 M pyrrole and 0.1 M NaCl. All the experiments were carried out at room temperature and were repeated at least three times and the plots shown are the average of these three experiments.

## Results and discussion

### Formation of PPy/s $\beta$ -CD

The anionic s $\beta$ -CD, with 7 to 11 anionic sites per molecule, provides the solution with a high conductivity and ionic strength. Therefore, it can be used without any supporting electrolyte. In order to compare the electropolymerisation of pyrrole in s $\beta$ -CD and in a chloride electrolyte, the concentrations of the two dopants were altered to give a constant solution conductivity. Typical data are shown in Fig. 1a, where the electropolymerisation is compared for the s $\beta$ -CD and chloride dopants, where the conductivity of the solutions was 5.0 mS cm<sup>-1</sup>. The onset of electropolymerisation occurs at about 0.50 V vs SCE in both systems. However, between 0.50 and 0.60 V vs SCE, higher currents are achieved in the presence of s $\beta$ -CD, with the current beginning to increase more rapidly at 0.55 V vs SCE. With the chloride system, similar current increases are only evident at a higher potential of 0.60 V vs SCE. However, in the vicinity of 0.75 V vs SCE, the rate of electropolymerisation is somewhat slower with s $\beta$ -CD with the slope of the plots at 77 mA V<sup>-1</sup> for PPy/Cl and 38 mA V<sup>-1</sup> for PPy/s $\beta$ -CD. These lower slopes may be connected to the slower diffusion of the large s $\beta$ -CD anions. The

early onset of electropolymerisation at approximately 0.50 V vs SCE for the s $\beta$ -CD suggests that the pyrrole is free and not included inside the cavity of the cyclodextrin. It has been reported that a shift of the anodic potential in the positive direction, during the electrochemical polymerisation of pyrrole in the presence of a neutral  $\beta$ -cyclodextrin, is due to the formation of an inclusion complex between the monomer and the CD [11]. This is not evident in Fig. 1a. Indeed, on recording <sup>1</sup>H NMR spectra for pyrrole in the absence and presence of an excess (six-fold) of s $\beta$ -CD in D<sub>2</sub>O, no change in the chemical shift was observed. Identical chemical shifts at  $\delta$  = 6.78 ppm (2H, s) and  $\delta$  = 6.23 ppm (2H, s) were seen in the absence and presence of s $\beta$ -CD. This indicates that the anionic pendants on the rim of the CD cavity prevent the host–guest complexation between s $\beta$ -CD and pyrrole. The mass–time curve recorded using EQCM at 0.70 V vs Ag|AgCl in 0.01 M s $\beta$ -CD and 0.1 M pyrrole is presented in the inset in Fig. 1a. There is an induction period of about 2–3 s before the mass begins to increase and then a linear increase in the mass is observed with increasing time, with a gradient of 0.1  $\mu$ g s<sup>-1</sup> ( $R^2$  = 0.998). This mass–time gradient increases with the concentration of pyrrole, s $\beta$ -CD and the applied potential; however, the ratio of the mass to charge remains at approximately 4.25  $\times 10^{-4}$  g C<sup>-1</sup>. This induction period depends on the rate of electropolymerisation and is no longer evident at 0.80 V vs SCE. It is probably related to the adsorption of the anionic cyclodextrin at the gold substrate. However, it is also possible that an inclusion complex is formed, or electrostatic interactions occur, between the anionic cyclodextrins and radical cations generated on oxidation of pyrrole. These interactions would reduce the rate of the radical coupling reactions. This will ultimately depend on the lifetime of the radical cations compared to the stability constant of any inclusion complex or ion pair formed.

The electropolymerisation and simultaneous redox activities of the polymer film formed in the presence of 0.01 M s $\beta$ -CD are shown in Fig. 1b. The characteristic broad waves are seen with the peak current for both the oxidation, at about -0.20 V vs SCE, and reduction, centered around -0.60 V vs SCE, increasing with cycle number. This

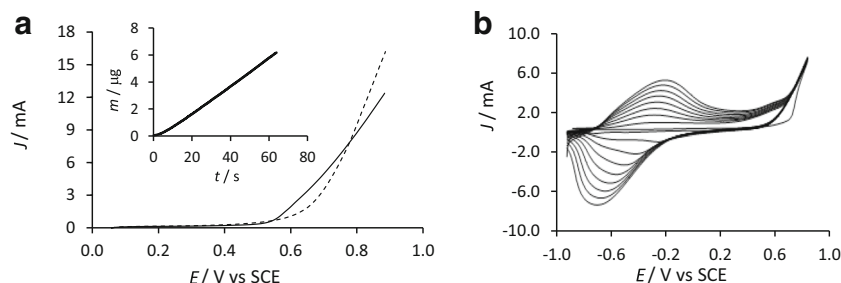


**Fig. 1** **a** Voltammogram for the oxidation of pyrrole in the presence of 0.2 M pyrrole with 0.01 M s $\beta$ -CD (—) and 0.10 M NaCl (---), inset shows the mass–time plot recorded at 0.70 V vs SCE in 0.01 M s $\beta$ -CD

and 0.1 M pyrrole. **b** Cyclic voltammogram recorded at 50 mV s<sup>-1</sup> during the formation of PPy/s $\beta$ -CD in 0.1 M pyrrole and 0.01 M s $\beta$ -CD

shows that increasing amounts of conducting PPy/s $\beta$ -CD are deposited. Very good reproducibility was obtained on forming the PPy/s $\beta$ -CD films and this is clearly illustrated in Fig. 2a where the data from three different experiments are presented for the formation of PPy/s $\beta$ -CD at 0.70 V vs SCE. There is very little variation in the currents or shape of the current–time plots. An initial rapid current decay is followed by a rise in the current before near constant currents are observed at longer polarisation times. This is consistent with the formation of a polymer monolayer, followed by continued three-dimensional growth. It is clearly evident that nearly identical currents are observed over the 15-s period. Furthermore, the time required to deposit the polymer to a charge density of 0.20 C cm<sup>-2</sup> was computed as 25.1  $\pm$  0.1 s, averaged over ten experiments, again indicating very good reproducibility. However, this high level of reproducibility was only achieved by preparing fresh solutions before each experiment.

The surface morphology of PPy/s $\beta$ -CD is shown in Fig. 2b for PPy/s $\beta$ -CD films formed to a charge density of 1.13 C cm<sup>-2</sup>, where the characteristic cauliflower morphology is evident. The cauliflower or globular structures range in size with some reaching diameters as high as 18  $\mu$ m, as shown in the inset in Fig. 2b. The micrographs shown in Fig. 2c, d were recorded for PPy/s $\beta$ -CD films formed to a final charge density of 0.35 and 0.09 C cm<sup>-2</sup>, respectively. It seems that as the thickness of the polymer decreases, this leads to the appearance of smaller globular particles, which agrees well with the

AFM study reported by Suarez and Compton for polypyrrole films doped with perchlorate and p-toluenesulfonate [24].

### Formation of PPy/CM $\beta$ -CD

A similar approach was employed to electrochemically synthesise PPy/CM $\beta$ -CD and again no supporting electrolyte was added. However, the concentration of pyrrole was increased to 0.3 M, and a higher applied potential of 0.80 V vs SCE was used; otherwise, the growth of the polymer was very slow. The CM $\beta$ -CD sodium salt has a lower degree of substitution with an average of 3.5 carboxylate groups on each CD. The conductivity of the CM $\beta$ -CD solution was measured as 3.10 mS cm<sup>-1</sup>, which is somewhat lower than the value obtained for the s $\beta$ -CD solution (5.0 mS cm<sup>-1</sup>), consistent with the lower number of anionic groups for the CM $\beta$ -CD. A typical current–time plot recorded during the formation of PPy/CM $\beta$ -CD is shown in Fig. 3a. On comparing these data to Fig. 2a, it is clear that the rate of electropolymerisation is significantly lower in the presence of the CM $\beta$ -CD anions. The current only begins to increase after about 40 s and then the rate of the current increase is low indicating a slow nucleation process followed by a slow growth of the polymer on the deposited PPy/CM $\beta$ -CD. The current only begins to increase after a 5-min period.

While the conductivity of the electropolymerisation solution will have an influence on the rate of electropolymerisation, the

**Fig. 2** **a** Current–time plots (three repeated experiments) for the electropolymerisation of pyrrole at 0.70 V vs SCE in 0.2 M pyrrole and 0.02 M s $\beta$ -CD and SEM micrographs of PPy/s $\beta$ -CD formed at 0.70 V vs SCE deposited to a charge density of **b** 1.13 C cm<sup>-2</sup>, **c** 0.35 C cm<sup>-2</sup>, and **d** 0.09 C cm<sup>-2</sup>

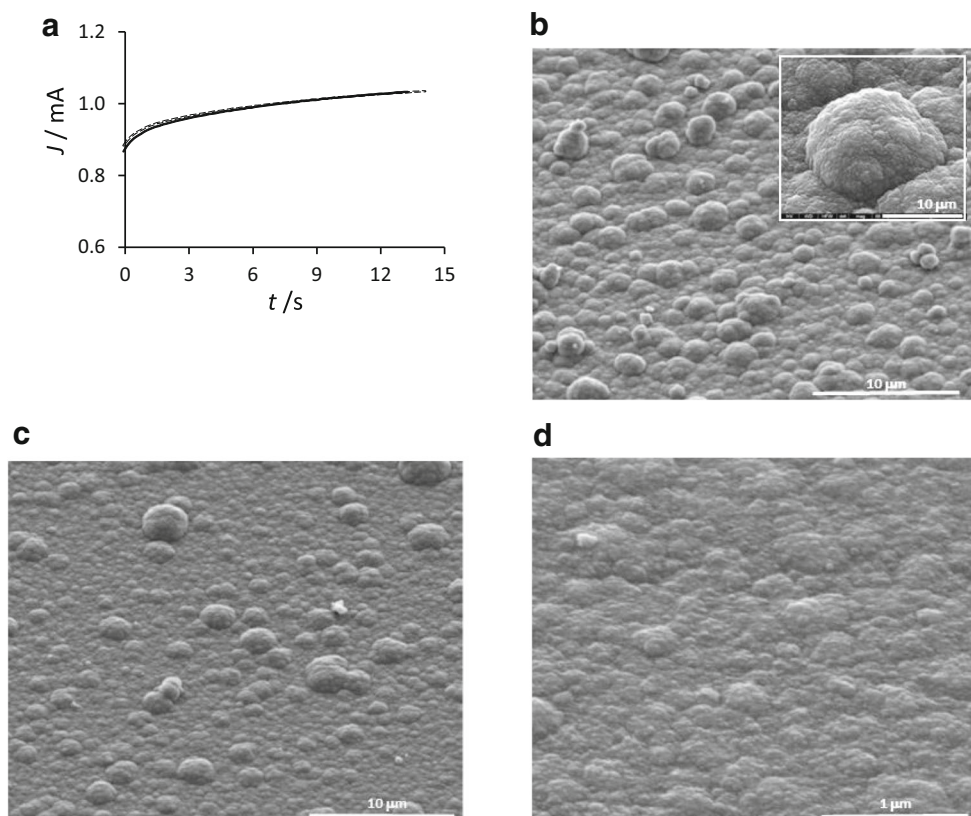
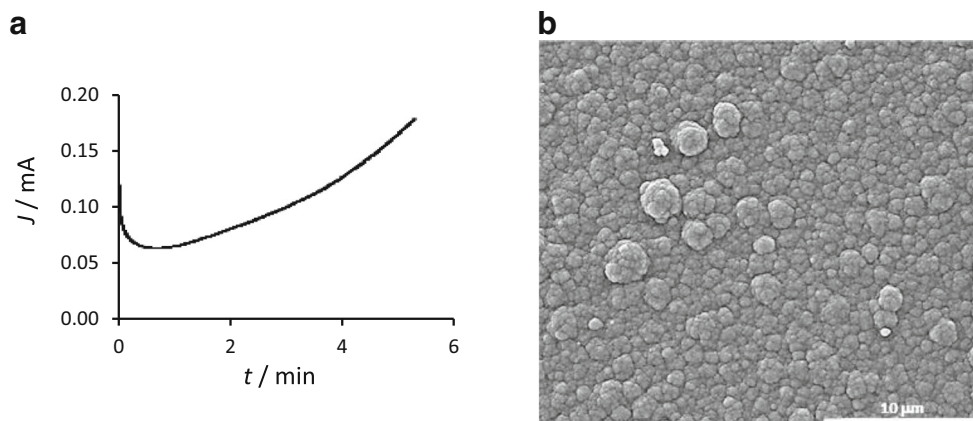


**Fig. 3** **a** Current–time plot for the electropolymerisation of pyrrole from a solution of 0.3 M pyrrole and 0.02 M CM $\beta$ -CD at 0.80 V vs SCE. **b** SEM micrograph of PPy/CM $\beta$ -CD deposited at 0.80 V vs SCE to a charge density of 1.13 C cm $^{-2}$



$pK_a$  value of the two pendants will have a greater influence. The  $pK_a$  of carboxylic acids is typically about 4.0, while the  $pK_a$  of acetic acid, which has a methyl group, is somewhat higher at 4.7. On the other hand, the  $pK_a$  value for  $H_2SO_3$  is 1.9. This clearly illustrates that the sulfonated pendant is difficult to protonate, while an equilibrium between the anionic carboxymethyl pendant and its corresponding neutral acid form will exist, as illustrated in Eq. 2.



An estimate of the % of anionic groups as a function of pH can be obtained using the well-known Henderson-Hasselbalch equation, Eq. 3. Using a value of 4.0 for the  $pK_a$ , about 55% of the pendants will be anionic at a pH of 4.4, but the % will decrease rapidly to only 5% at a pH of 3.0. It is well known that protons are released during the electropolymerisation reaction. The degree of acidification depends on the rate of electropolymerisation and interfacial pH values as low as 3.0 have been reported in the presence of perchlorate and chloride anions [25]. Therefore, as the interfacial pH decreases, the concentration of the anionic pendants will decrease, and as no other dopants are available, the rate of electropolymerisation will be slow, consistent with the data presented in Fig. 3a. Furthermore, as more of the pendants become neutral, the solubility of the cyclodextrin in the solution phase will decrease.

$$\%[-COO^-] = \frac{100}{1 + 10^{(pK_a - pH)}} \quad (3)$$

The surface morphology of the PPy/CM $\beta$ -CD is shown in Fig. 3b, where the globular and cauliflower structures are again evident. The globular structures appear to be smaller in diameter compared to the morphology seen with PPy/s $\beta$ -CD. Although PPy/CM $\beta$ -CD was deposited to the same charge density as PPy/s $\beta$ -CD, the rate of electropolymerisation is considerably slower and this will have an influence on the surface

morphology [24]. These data clearly show that polypyrrole can be doped with CM $\beta$ -CD, but the rate of electropolymerisation is low and to maintain the CD in solution, low rates of electropolymerisation are desirable; otherwise, the interfacial solution becomes too acidic and the cyclodextrins will become insoluble and precipitate within the polymer matrix.

### Redox and ion exchange properties of PPy/s $\beta$ -CD and PPy/CM $\beta$ -CD

The cyclic voltammograms recorded for PPy/s $\beta$ -CD and PPy/CM $\beta$ -CD in 0.10 M NaCl are shown in Fig. 4a, b, respectively. In Fig. 4a, the first cycle is shown and compared to the voltammograms recorded with higher cycles, where steady-state conditions are achieved. There is a pronounced reduction wave for the first cycle centered at approximately  $-0.56$  V vs SCE, which corresponds to the incorporation of  $Na^+$  from the electrolyte solution. This is consistent with the large and bulky size of the S $\beta$ -CD which is not expelled during reduction of the polymer. Instead, reduction is accompanied by the ingress of  $Na^+$  cations from the NaCl electrolyte. The corresponding anodic peak at about  $-0.32$  V vs SCE represents the expulsion of cations. It is also evident that this behaviour, although slightly suppressed, is observed for the successive cycles, indicating that the ionic exchange is reversible. In Fig. 4b, the steady-state voltammogram is shown for PPy/CM $\beta$ -CD. The reduction wave is centred at approximately  $-0.40$  V vs SCE, about 160 mV higher than that seen with PPy/s $\beta$ -CD. This potential shift is probably related to the lower thickness of the PPy/CM $\beta$ -CD. It is well known that the appearance and shape of the redox waves depend on the thickness of the polymer films [26]. Indeed, on reducing the thickness of the PPy/s $\beta$ -CD, the reduction peak became less broad shifting the peak potential closer to the value adopted by the PPy/CM $\beta$ -CD (illustrated in Fig. 4c). However, the PPy/CM $\beta$ -CD film is more difficult to oxidise with oxidation extending from about  $-0.20$  to  $0.70$  V vs SCE, while oxidation of the PPy/s $\beta$ -CD begins at about  $-0.40$  V vs SCE. It is also clear that the

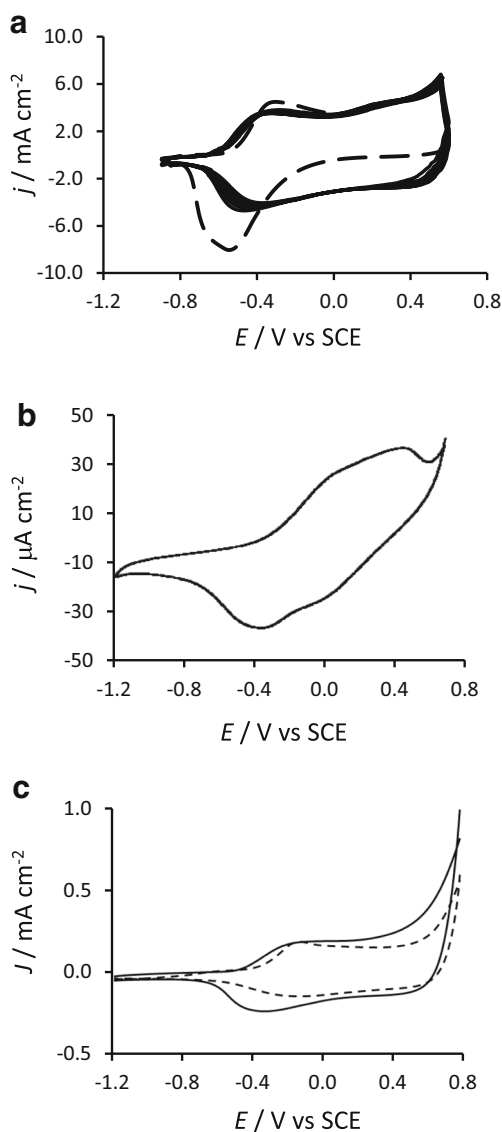


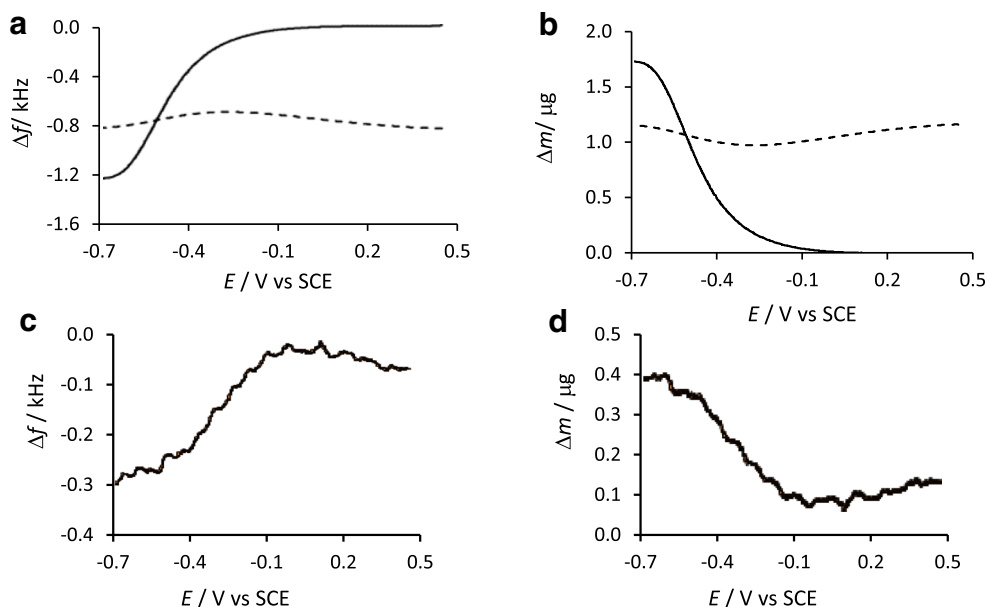
**Fig. 4** Cyclic voltammograms recorded at  $50 \text{ mV s}^{-1}$  in  $0.10 \text{ M NaCl}$  for **a** PPy/s $\beta$ -CD deposited at  $0.70 \text{ V vs SCE}$  to a charge of  $0.8 \text{ C cm}^{-2}$ , first cycle (---) and remaining cycles (—), **b** PPy/CM $\beta$ -CD deposited at  $0.80 \text{ V vs SCE}$  to a charge of  $0.2 \text{ C}$  (cycle 15) and **c** PPyCl (---) and PPy/s $\beta$ -CD (—) deposited at  $0.70 \text{ V vs SCE}$  to a charge of  $0.2 \text{ C}$  (cycles 15)

currents are considerably higher for the PPy/s $\beta$ -CD, indicating a higher capacitance. The high capacitance of PPy/s $\beta$ -CD may be associated with the large number of anionic pendants on the CD cavity. As each CD cavity has an average of nine sulfonated groups, it is unlikely that these are all involved in the doping process. This would not only place considerable strain on the CD but also on the polymer matrix. Instead, some of these groups are probably free and the charge is compensated by  $\text{Na}^+$  cations from the electrolyte. Indeed, Naoi and co-workers [27], in studying the doping of polypyrrole sulfonated naphthalene, concluded that the PPy-trisulfonate doped films possessed free sulfonated groups without any charge compensation.

The low electroactivity observed with the PPy/CM $\beta$ -CD film may be due to the lower number of anionic pendants; however, it is also possible that the precipitation of small amounts of insoluble CM $\beta$ -CD occurs during electropolymerisation. In Fig. 4c, steady-state voltammograms are shown for PPy/s $\beta$ -CD and PPy/Cl formed to a charge density of  $0.20 \text{ C cm}^{-2}$  which correspond to the charge used to deposit PPy/CM $\beta$ -CD. It is clear that the currents obtained with these polymer films, reaching about  $200 \mu\text{A cm}^{-2}$  between  $-0.20$  and  $0.30 \text{ V vs SCE}$ , are significantly higher than that obtained with the PPy/CM $\beta$ -CD film, where the maximum current is only  $40 \mu\text{A cm}^{-2}$ . While the fixed charge may not give the same polymer thickness for the PPy/s $\beta$ -CD and PPy/CM $\beta$ -CD systems, the difference in the voltammograms is too large to be connected to variations in the film thickness or porosity. This was further checked by comparing the two polymers formed to a final current of  $1.0 \text{ mA}$ . Again, a similar result was obtained when the polymers were cycled in  $0.1 \text{ M NaCl}$ ; the PPy/CM $\beta$ -CD showed poor electroactivity. This lends support to the idea that small amounts of insoluble CM $\beta$ -CD may be formed due to the protonation of the ionised  $\beta$ -CD, giving the poorly soluble neutral CD.

These exchange processes are further evident in Fig. 5a, b where the mass changes obtained using EQCM measurements are shown for PPy/s $\beta$ -CD. The polymer films were cycled in a  $0.1 \text{ M NaCl}$  solution, from  $0.60$  to  $-1.2 \text{ V vs Ag|AgCl}$ , at a scan rate of  $10 \text{ mV s}^{-1}$ . Steady-state conditions for the ionic exchange were achieved after ten cycles. On initial reduction of the polymer, an increase in the mass is observed, starting at about  $-0.10 \text{ V vs Ag|AgCl}$  and becoming more rapid at about  $-0.50 \text{ V vs Ag|AgCl}$ , which is in good agreement with the data obtained for the bulk polymer, Fig. 4a. This is consistent with the insertion of  $\text{Na}^+$  to maintain electroneutrality. Clearly, the first and tenth cycles have different shapes. The tenth cycle indicates mixed cation and anion exchange properties. A small decrease in mass is observed on reducing the PPy/s $\beta$ -CD from  $0.50$  to  $-0.10 \text{ V vs Ag|AgCl}$ , which is consistent with the loss of  $\text{Cl}^-$ . On the other hand, an increase in mass is observed on reduction of the PPy/s $\beta$ -CD from  $-0.30$  to  $-0.70 \text{ V vs Ag|AgCl}$ , which can be attributed to the ingress of  $\text{Na}^+$  to balance the anionic s $\beta$ -CD. This apparent transition from cation exchange to mixed ion exchange may be due to the large ingress of  $\text{Na}^+$  observed on initial reduction. Some of the  $\text{Na}^+$  cations become trapped within the polymer matrix, leading to a subsequent ingress of  $\text{Cl}^-$  anions to maintain electroneutrality as the polymer is oxidised [28]. Indeed, the  $\Delta\text{mass}$ , at the end of the redox cycling, is positive, signifying that some of the ionic species injected into the polymer are not subsequently lost. In Fig. 5c, d, the first cycle data are shown for PPy/CM $\beta$ -CD. The traces are somewhat noisy as the change in mass is small and close to the detection limit. However, it is clear that an increase in mass is observed as the PPy/CM $\beta$ -CD

**Fig. 5** EQCM data recorded on cycling at  $10 \text{ mV s}^{-1}$  in  $0.1 \text{ M NaCl}$  **a** frequency–potential **b** and mass–potential plots for PPy/s $\beta$ -CD, 1st reduction cycle (—), 10th reduction cycle (…), **c** frequency–potential and **d** mass–potential plots for PPy/CM $\beta$ -CD, 1st reduction cycle



is reduced. Although, the PPy/s $\beta$ -CD and PPy/CM $\beta$ -CD films were deposited to the same charge, there is a much lower mass change seen with the PPy/CM $\beta$ -CD. This is consistent with the lower electroactivity of the PPy/CM $\beta$ -CD seen in the steady-state voltammograms, Fig. 4b.

### Uptake of $\text{Na}^+$ and $\text{H}_2\text{O}$ at PPy/s $\beta$ -CD

The PPy/s $\beta$ -CD which is easily synthesised, as the sulfonated pendants are difficult to protonate, and shows good electroactivity was studied further to obtain more details on its redox processes and capacitance. Using EQCM, the uptake of  $\text{Na}^+$  and water molecules was studied. In order to apply the Sauerbrey equation to this analysis, the film must behave as a rigid and perfectly elastic layer. This rigid film approximation is normally valid when thin polymer films are used. In an attempt to avoid viscoelasticity complications, films were grown to a maximum charge density of  $0.10 \text{ C cm}^{-2}$ . According to Faraday's law, the mass,  $m$ , is a linear function of charge, Eq. 4, where  $q$  is the charge,  $n$  represents the number of electrons transferred and  $j$  is the current density. Therefore, a plot of the mass as a function of the charge consumed during polymerisation should be linear if these viscoelasticity complications are absent. As highlighted in Fig. 6a, linear plots ( $R^2 = 0.999$ ) were obtained for the deposition of PPy/Cl and PPy/s $\beta$ -CD deposited to a charge density of  $0.12 \text{ C cm}^{-2}$  ( $25 \text{ mC}$ ), which is beyond the maximum value of  $0.10 \text{ C cm}^{-2}$  used in this analysis, and hence these polymer films were assumed to be rigid. Another aspect that is clearly evident from the frequency–charge and mass–charge plots is the higher mass deposited for PPy/s $\beta$ -CD which is approximately  $1.06 \times 10^{-5} \text{ g}$  in comparison to the mass of  $7.06 \times 10^{-6} \text{ g}$  for PPy/Cl. This gives mass–charge slopes of  $4.25 \times 10^{-4}$  for

PPy/s $\beta$ -CD and  $2.82 \times 10^{-4} \text{ g C}^{-1}$  for PPy/Cl, which are consistent with the higher mass of the s $\beta$ -CD dopant.

$$q = \int_0^t j \, dt = mnF \quad (4)$$

Assuming that only  $\text{Na}^+$  takes part in the charge balance, then the mass change on reduction of the polymer can be calculated using Eq. 5. This theoretical mass associated with  $\text{Na}^+$  exchange was calculated and is plotted in Fig. 6b together with the experimental data for the first cycle. Clearly, the mass–charge plot for the experimental data is divided into two linear segments. At low charge values, which correspond to the potential interval from  $0.50 \text{ V}$  to about  $-0.10 \text{ V}$  vs Ag|AgCl, the charge is carried by species with a molecular mass lower than  $\text{Na}^+$ . This is probably related to the ingress of protons [29]. At the higher charges, which correspond to more negative potentials, the mass carrying the charge is higher than  $\text{Na}^+$ . This can be explained in terms of water incorporation, where the water accompanies the  $\text{Na}^+$  forming a solvation shell around the  $\text{Na}^+$  cation. The ingress of the solvated  $\text{Na}^+$  is not observed at the more positive potentials, suggesting that this phenomenon may be related to a change in the porosity of the reduced PPy/s $\beta$ -CD [24].

$$m = \frac{Mw}{F} Q_M \quad (5)$$

The significance of the solvation shell involved in the sodium exchange was further investigated by assuming that all the water incorporated is associated with the  $\text{Na}^+$ . In this case, the variation of mass,  $\Delta m$ , during reduction of the polymer is

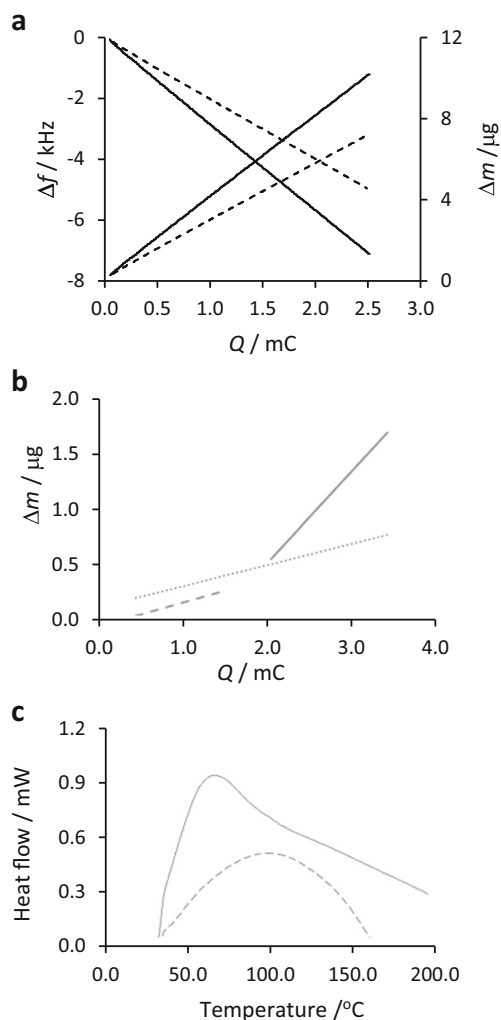


**Fig. 6** **a** EQCM data recorded during the formation of PPY/Cl (---) and PPY/sβ-CD(—) at 0.70 V vs SCE in 0.2 M pyrrole and 0.02 M sβ-CD, **b** Mass-charge plot for the theoretical (...) and experimental (—, - - -) redox activity of PPY/sβ-CD films cycled at 10 mV s<sup>-1</sup> in 0.1 M NaCl and **c** DSC thermogram of PPY/sβ-CD reduced in 0.10 M NaCl at -0.60 V vs SCE for 30 min (—) and in the oxidised state at 0.70 V vs SCE (---)

given by the mass of the sodium and water molecules, as described in Eq. 6, where  $M_{w_{Na^+}}$  and  $M_{w_{H_2O}}$  represent the molecular mass of  $Na^+$  and  $H_2O$ , respectively, while  $\xi$  corresponds to the number of moles. The charge,  $q$ , associated with the movement of the cation,  $Na^+$ , is given by Eq. 7, where  $F$  is Faraday's constant. Using  $h$  to represent the hydration number, Eq. 8, it is possible to write Eq. 9, where  $h$  is expressed in terms of mass and charge. On fitting the EQCM data for the PPY/sβ-CD polymer to Eq. 8, the  $h$  value was found to be 4.08. This value is in good agreement with the work reported by Torresi et al. [30] who concluded that an average of 4.5 water molecules accompanied the ingress of  $Na^+$  on reduction of polypyrrole doped with dodecylbenzenesulfonate.

$$\Delta m = M_{w_{Na^+}} \xi_{Na^+} + M_{w_{H_2O}} \xi_{H_2O} \quad (6)$$

$$q = F \xi_{Na^+} \quad (7)$$

$$\xi_{H_2O} = h \xi_{Na^+} \quad (8)$$

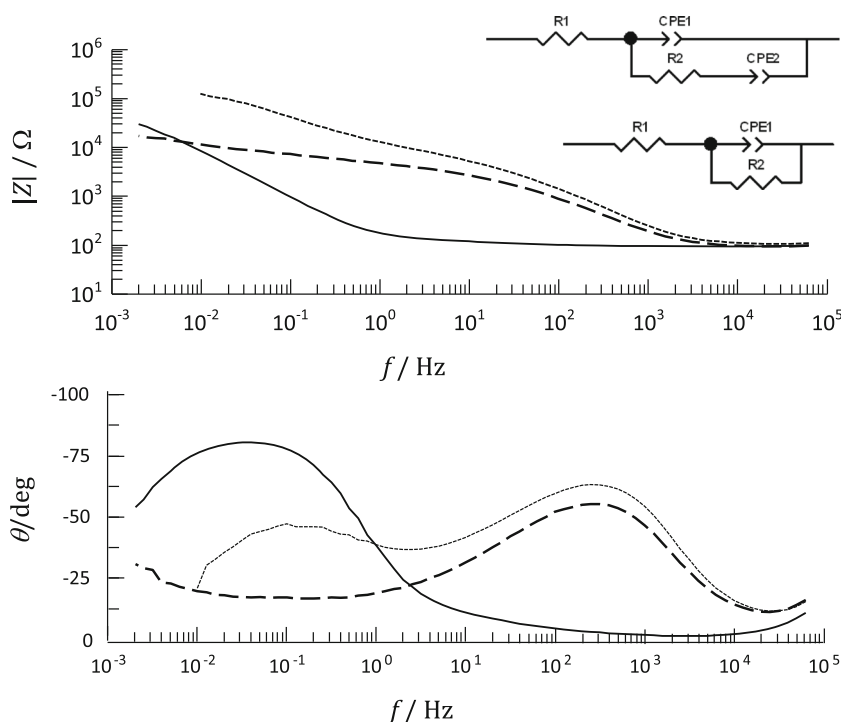
$$h = \frac{F \Delta m}{q M_{w_{H_2O}}} - \frac{M_{w_{Na^+}}}{M_{w_{H_2O}}} \quad (9)$$

The swelling of the polymer and incorporation of water molecules during reduction of the PPY/sβ-CD was confirmed using DSC analysis. Reduced and oxidised samples of PPY/sβ-CD were dried in an oven, at 50 °C for 96 h prior to recording the DSC thermograms. On heating the samples, the amount of water lost from the reduced polymer was significantly higher, as evident from Fig. 6c. While this does not provide sufficient evidence for different water contents as the oxidised and reduced PPY/sβ-CD films have different polymer backbones, with the reduced polymer enriched in  $Na^+$  cations, these results corroborate the incorporation of water within the polymer matrix as the films are reduced. Furthermore, it is evident that the oxidised PPY/sβ-CD contains water molecules. As the polymer samples were heated at 50 °C for 96 h, any residual water is removed and the endothermic peak at about 100 °C can be attributed to strongly bound water. It appears that the water molecules incorporated with the intake of  $Na^+$  are weakly bound and the endothermic peak is shifted to a lower temperature. The broad and unsymmetrical shape of this endothermic peak suggests that both strongly bound and weakly bound water are present in the reduced PPY/sβ-CD.

### Capacitance and stability of PPY/sβ-CD

The voltammograms recorded for PPY/sβ-CD (Fig. 4) are consistent with a high capacitance. A complementary study on the ability of the PPY/sβ-CD film to store charge was performed using electrochemical impedance spectroscopy. Representative impedance plots, presented as Bode plots, are shown in Fig. 7 for PPY/sβ-CD films under open-circuit conditions (approximately 0.25 V vs SCE), and polarised at -0.80 and 0.70 V vs SCE. In all cases, the data were recorded following a 60-min polarisation period at the desired potential to ensure steady-state conditions were achieved. This was further tested by recording the impedance from high to low frequencies and then from low to high frequencies and no hysteresis was observed following this pre-polarisation period. Clearly, the applied potential, and in turn the oxidation state of the polymer, has a significant influence on the impedance response. The impedance profile changes from a simple one-time constant model when the polymer is reduced to a two-time constant model when the polymer is oxidised at 0.70 V vs SCE. These data were fit to the equivalent circuits depicted in Fig. 7. A simple Randles cell was used to model the data

**Fig. 7** Bode plots and circuit elements for PPy/sβ-CD recorded in 0.10 M NaCl using a perturbation amplitude of 5.0 mV, measured at open-circuit potential (—), at -0.80 V vs SCE (---) and 0.70 V vs SCE (⋯⋯)



when the polymer was reduced, or partially reduced, while a second CPE was added for the oxidised polymer. In these circuits, R1 represents the solution resistance, R2 represents the charge-transfer resistance, while CPE1 and CPE2 are constant phase elements.

The impedance responses of the PPy/sβ-CD and PPy/Cl films were recorded as a function of the applied potential to probe the capacitive properties of the polymers at different levels of oxidation and reduction. The constant phase element CPE1 (Randles cell) with an exponent  $n = 0.93$  was used to represent the capacitance of the reduced or partially reduced polymer, while CPE2 with  $n = 1.0$  was employed to give an estimate of the capacitance of the oxidised polymer. The  $n$  value for CPE1 varied from 0.71 to 0.73 for the oxidised polymer and therefore it was not used to represent capacitance. The data presented in Fig. 8 show the capacitance plotted as a function of the applied potential for PPy/sβ-CD and PPy/Cl. It is clearly evident that the capacitance is higher for the PPy/sβ-CD films, reaching a value of about  $6.0 \text{ mF cm}^{-2}$ . The capacitance is essentially constant between 0.60 and  $-0.60 \text{ V vs SCE}$ ; however, there is a considerable drop in the capacitance, as the potential is increased above  $0.60 \text{ V vs SCE}$ , reaching values as low as  $0.018 \text{ mF cm}^{-2}$  at  $0.70 \text{ V vs SCE}$ . This decay in the capacitance is related to the over-oxidation of the polypyrrole matrix. As the potential is reduced further to  $-0.80 \text{ V vs SCE}$ , there is a reduction in the capacitance. This is consistent with the formation of the reduced  $\text{PPy}^0/\text{s}\beta\text{-CD Na}^+$  film. This transition is observed at about  $-0.50 \text{ V vs SCE}$  which is in good agreement with the voltammetry data presented in Fig. 4a. The PPy/sβ-CD film

can be readily reversed between the reduced and the oxidised or partially oxidised states by switching the applied potential between  $-0.80$  and  $0.50 \text{ V vs SCE}$  and nearly identical capacitance values are recorded prior to and after reduction, indicating very good reversibility. As the sβ-CD is a large and immobile dopant, these potential variations give rise to the insertion and expulsion of sodium cations and their associated water molecules and chloride anions from the electrolyte solution, as illustrated in Fig. 5. On comparing these data with the PPy/Cl film, it is seen that the PPy/sβ-CD is over-oxidised at a lower potential of about  $0.60 \text{ V vs SCE}$  compared to  $0.70 \text{ V vs SCE}$  for the PPy/Cl. The reduced polymer,  $\text{PPy}^0$ , is formed on reduction of PPy/Cl to give low

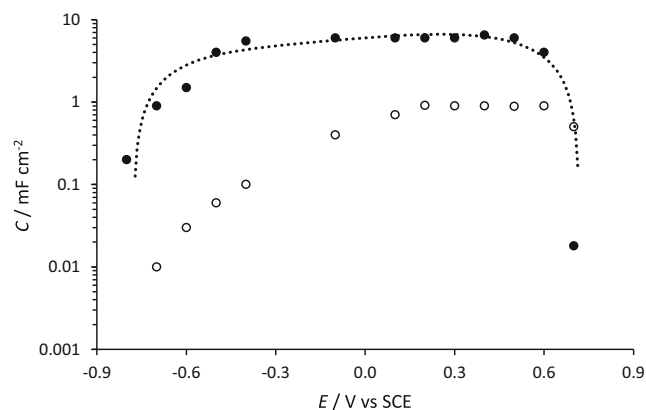


**Fig. 8** Capacitance plotted as a function of potential for PPy/sβ-CD (●) and PPy/Cl (○) recorded in 0.1 M NaCl. Error in the fitted circuit element was 2.1%

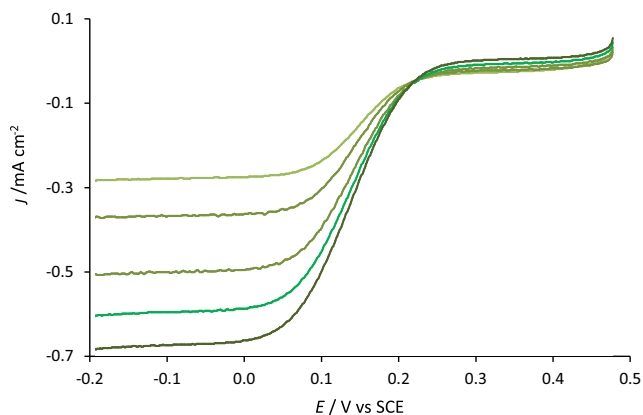


**Fig. 9** RDV data recorded in  $5.0 \times 10^{-3}$  M  $\text{K}_3\text{Fe}(\text{CN})_6$  and 0.10 M NaCl at 250, 500, 1000, 1250, 1500 rpm, at a scan rate of  $5 \text{ mV s}^{-1}$ , at PPy/s $\beta$ -CD

capacitance values, while the higher values obtained for the PPy/s $\beta$ -CD are associated with the formation of PPy<sup>o</sup>/s $\beta$ -CD<sup>-</sup>Na<sup>+</sup>.

The specific capacitance was calculated using the mass of the polymer obtained from EQCM data. The mass–charge slope of  $4.25 \times 10^{-4} \text{ g C}^{-1}$ , obtained from Fig. 6a, was used with the charge consumed during formation of the polymer to compute the mass of the PPy/s $\beta$ -CD as 10.6  $\mu\text{g}$ . Using the capacitance of  $6 \text{ mF cm}^{-2}$  obtained in Fig. 8, this gives a specific capacitance of  $71 \text{ F g}^{-1}$ . The thickness of the PPy/s $\beta$ -CD film was measured as  $430 \pm 30 \text{ nm}$  using a Tencor profilometer. The surface area of the polymer was estimated using the ferricyanide redox couple as  $0.1397 \text{ cm}^2$ , which corresponds to an increase of 11% compared to the geometric surface area ( $0.1257 \text{ cm}^2$ ). This gives a volume of  $6.01 \times 10^{-6} \text{ cm}^3$  and a volume to charge ratio of  $2.4 \times 10^{-4} \text{ cm}^3 \text{ C}^{-1}$ , which compares well to the values reported by Holzhauser and Bouzek, which range from  $1.86 \times 10^{-4}$  to  $3.0 \times 10^{-4} \text{ cm}^3 \text{ C}^{-1}$  depending on the dopant [31]. Using the mass and computed volume, the density of the polymer was estimated at  $1.76 \text{ g cm}^{-3}$ . This is somewhat higher than the value of  $1.5 \text{ g cm}^{-3}$  [31] that is typically used as the density of polypyrrole and this is consistent with the high mass of the  $\beta$ -CD dopant. Although, the  $\beta$ -CD is large and bulky and will probably give a porous polymer with a high volume, the high

mass of the dopant appears to have more influence on the density.

### Electron transfer at the PPy/s $\beta$ -CD modified electrode

Potassium ferricyanide,  $\text{K}_3\text{Fe}(\text{CN})_6$ , was employed to study the rate of electron transfer at the PPy/s $\beta$ -CD interface. Rotating disc voltammetry (RDV) was used and the data were fitted to the Koutecky–Levich relationship to obtain the rate constant,  $k$ , Eq. 10. In this analysis,  $i_L$  is the limiting current,  $n$  is the number of electrons transferred,  $F$  is Faraday’s constant,  $k$  is the rate constant,  $D$  is the diffusion coefficient,  $\nu$  is the kinematic viscosity,  $A$  is the surface area,  $c$  is the concentration of the electroactive species and  $\omega$  is the rotational rate. The diffusion coefficient was evaluated by applying the Levich equation, Eq. 11.

$$\frac{1}{i_L} = \frac{1}{n F A k c} + \frac{1.61}{n F A \nu^{-1/6} D^{2/3} c \omega^{1/2}} \quad (10)$$

$$i_L = 0.621 n F A D^{2/3} \nu^{-1/6} c \omega^{1/2} \quad (11)$$

Typical RDV data collected using a scan rate of  $5 \text{ mV s}^{-1}$  are shown in Fig. 9. Limiting currents were observed from about 0.0 to  $-0.20 \text{ V vs SCE}$  and these increased with the rotation rate. Levich plots, where the limiting current was measured at  $-0.10 \text{ V vs SCE}$ , are presented in Fig. 10a for unmodified GC, PPy/Cl and PPy/s $\beta$ -CD. These show good linearity. Diffusion coefficients of  $6.47 \times 10^{-6}$ ,  $6.21 \times 10^{-6}$  and  $5.3 \times 10^{-6} \text{ cm}^2 \text{ s}^{-1}$  for PPy/s $\beta$ -CD, PPy/Cl and GC, respectively, were obtained from these data. The somewhat higher values recorded with the polymer system are probably connected with a larger surface area. The inverse of the limiting current plotted as a function of the inverse of the square root of the rotation rate is shown in Fig. 10b. The linear plot for PPy/s $\beta$ -CD is very similar to that obtained for the PPy/Cl system, with similar rate constants. The rate constants were calculated as  $3.73 \times 10^{-2}$ ,  $3.32 \times 10^{-2}$  and  $3.63 \times 10^{-2} \text{ cm s}^{-1}$  for PPy/s $\beta$ -CD, PPy/Cl and GC, respectively. At these slow

**Fig. 10** **a** Levich and **b** Koutecky–Levich plots recorded in  $5.0 \times 10^{-3}$  M  $\text{K}_3\text{Fe}(\text{CN})_6$  in 0.10 M NaCl, recorded at  $5 \text{ mV s}^{-1}$  for a GC electrode ( $\blacklozenge$ ) PPy/s $\beta$ -CD ( $\bullet$ ) and PPy/Cl ( $\circ$ ) modified electrodes

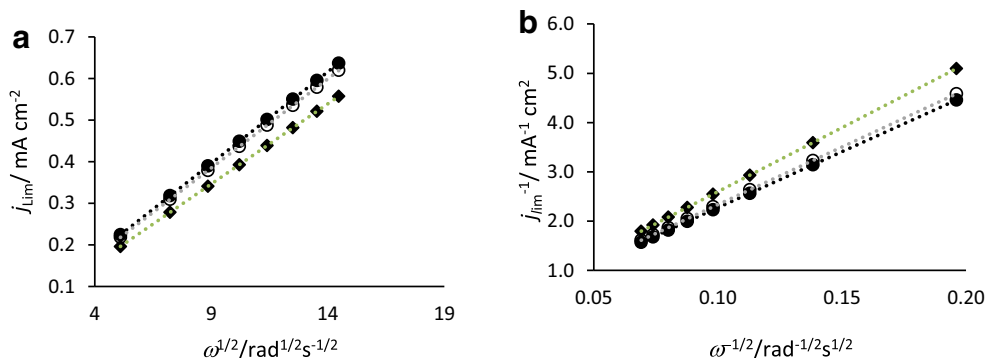


**Table 1** Ratio of peak currents for the electrochemistry of 5 mM  $K_3Fe(CN)_6$  in 0.1 M NaCl cycled between  $-0.20$  and  $0.50$  V vs SCE as a function of scan rate

Scan rate/ $mV s^{-1}$	$j_{ox}/j_{red}$		
	PPy/s $\beta$ -CD	GC	PPy/Cl
25	0.94	1.01	0.93
50	0.94	0.88	0.93
75	0.93	0.86	0.87
100	0.91	0.83	0.73
125	0.90	0.82	0.54
150	0.88	0.80	0.38

scan rates, Nernstian equilibrium is achieved and the rate constants for the three substrates are very close. However, at higher scan rates, kinetic limitations were evident. At a scan rate of  $50 mV s^{-1}$ , the Levich plots no longer pass through the origin for the PPy/s $\beta$ -CD and PPy/Cl modified electrodes. These results show that the electron transfer process is only slightly inhibited by the presence of the polymer and the presence of the large and bulky s $\beta$ -CD dopant does not give rise to any significant reduction in the rate of electron transfer.

The reversibility of the ferricyanide redox couple was also studied using cyclic voltammetry and compared for the unmodified GC, PPy/Cl and PPy/s $\beta$ -CD modified electrodes. Data obtained on computing the ratio,  $j_{ox}/j_{red}$ , are summarised in Table 1. The  $j_{ox}/j_{red}$  ratios obtained with the PPy/s $\beta$ -CD films are approximately 0.9 for scan rates from 25 to  $150 mV s^{-1}$ , while much lower values are obtained with the PPy/Cl polymer system. Indeed, the ratios obtained for the PPy/s $\beta$ -CD modified electrodes compare very well with the unmodified GC electrode, indicating that the presence of the large s $\beta$ -CD dopant does not inhibit electron transfer.

## Conclusions

Polypyrrole was formed in the presence of s $\beta$ -CD to generate highly conducting PPy/s $\beta$ -CD films, while less conducting PPy/CM $\beta$ -CD films were achieved. This highlights the role of the anionic pendants during electropolymerisation. While the conductivities of the CM $\beta$ -CD and s $\beta$ -CD solutions were relatively high at  $3.10$  and  $5.0 mS cm^{-1}$ , respectively, in near neutral solution, the carboxylate groups are protonated to give the neutral carboxylic acid as the solution becomes acidified at the electrode–solution interface. On the other hand, the sulfonated groups are considerably more difficult to protonate and remain as anions in acidic solutions. This solution equilibrium, with the weak carboxylic acid/carboxylate equilibrium system, leads to a low rate of electropolymerisation as the

anions are converted to the neutral CD at the electrode–solution interface.

**Acknowledgements** This work was financially funded by the Irish Research Council for Science, Engineering and Technology (IRCSET) Ireland and Science Foundation Ireland (SFI).

**Publisher's Note** Springer Nature remains neutral with regard to jurisdictional claims in published maps and institutional affiliations.

## References

- Janata J, Josowicz M (2003) Conducting polymers in electronic chemical sensors. *Nature Mater* 2(1):19–24
- Gurunathan K, Murugan A, Vadivel MR, Mulik UP, Amalnerkar DP (1999) Electrochemically synthesized conducting polymeric materials for applications towards technology in electronics, optoelectronics and energy storage devices. *Mater Chem Phys* 61(3): 173–191
- Weidlich C, Mangold K-M, Juetner K (2005) Continuous ion exchange process based on polypyrrole as an electrochemically switchable ion exchanger. *Electrochim Acta* 50(25-26):5247–5254
- Akieh MN, Price WE, Bobacka J, Ivaska A, Ralph SF (2009) Ion exchange behaviour and charge compensation mechanism of polypyrrole in electrolytes containing mono-, di- and trivalent metal ions. *Synth Met* 159(23-24):2590–2598
- Chen Y, Song L, Chen Z, Zhang L, Wu W (2015) Morphology and properties of polypyrrole/cyclodextrin nanowires using molecular templates. *Des Monomers Polym* 18(1):35–41
- Chauke VP, Maity A, Chetty A (2015) High-performance towards removal of toxic hexavalent chromium from aqueous solution using graphene oxide–alpha cyclodextrin–polypyrrole nanocomposites. *J Mol Liq* 211:71–77
- Hong S, Li Z, Li C, Dong C, Shuang S (2018)  $\beta$ -Cyclodextrin grafted polypyrrole magnetic nanocomposites toward the targeted delivery and controlled release of doxorubicin. *Appl Surf Sci* 427: 1189–1198
- Hu J, Wu X, Zeng W (2011) Formaldehyde sensor based on polypyrrole/ $\beta$ -cyclodextrin. *J Control Release* 152:e211–e213
- Arjomandi J, Holze R (2006) Spectroelectrochemistry of conducting polypyrrole and poly(pyrrole-cyclodextrin) prepared in aqueous and nonaqueous solvents. *J Solid State Electrochem* 11:1093–1100
- Izaoumen N, Bouchta D, Zejli H, El MK, Stalcup MA, Temsamani RK (2005) Electrosynthesis and analytical performances of functionalized poly (pyrrole/ $\beta$ -cyclodextrin) films. *Talanta* 66(1):111–117
- Storsberg J, Ritter H, Pielartzik H, Groenendaal L (2000) Cyclodextrins in polymer synthesis: supramolecular cyclodextrin complexes of pyrrole and 3,4-ethylenedioxythiophene and their oxidative polymerization. *Adv Mater* 12(8):567–569
- Lee C-Y, Hsu D-Y, Prasanna A, Kalaivani R, Hong P-D (2016) Facile synthesis of hexagonal-shaped polypyrrole self-assembled particles for the electrochemical detection of dopamine. *Appl Surf Sci* 363:451–458
- Shang S, Zeng W, Tao X-M (2012) Fabrication of conducting polypyrrole/ $\beta$ -cyclodextrin nano- and micro-spheres using molecular templates. *RSC Adv* 2(11):4675–4682
- Fritea L, Gorgy K, Le Goff A, Alan PA, Galmiche L, Săndulescu R, Cosnier S (2016) Fluorescent and redox tetrazine films by host-guest immobilization of tetrazine derivatives within poly(pyrrole- $\beta$ -cyclodextrin) films. *J Electroanal Chem* 781:36–40

15. Lagrost C, Chane-Ching KI, Lacroix J-C, Aeiyaeh S, Jouini M, Lacaze PC, Tanguy J (1999) Host-guest complexation: a convenient route to polybithiophene composites by electrosynthesis in aqueous media. Synthesis and characterization of a new material containing cyclodextrins. *J Mater Chem* 9(1999):2351–2358
16. Tamsamani KR, Mark HB Jr, Kutner W, Stalcup AM (2002) A simple one-step electrosynthesis of poly(pyrrole-sulfated  $\beta$ -cyclodextrin) films. *J Solid State Electrochem* 6(6):391–395
17. Bidan G, Lopez C, Mendes-Viegas F, Vieil E, Gabelle A (1995) Incorporation of sulfonated cyclodextrins into polypyrrole: an approach for the electro-controlled delivering of neutral drugs. *Biosens Bioelectron* 10(1-2):219–229
18. Reece DA, Ralph SF, Wallace GG (2005) Metal transport studies on inherently conducting polymer membranes containing cyclodextrin dopants. *J Membr Sci* 249(1-2):9–20
19. Harley CC, Rooney AD, Breslin CB (2010) The selective detection of dopamine at a polypyrrole film doped with sulfonated  $\beta$ -cyclodextrins. *Sensors Actuators B Chem* 150(2):498–504
20. Hamilton A, Breslin CB (2014) The development of a highly sensitive urea sensor due to the formation of an inclusion complex between urea and sulfonated- $\beta$ -cyclodextrin. *Electrochim Acta* 125:250–257
21. Hamilton A, Breslin CB (2014) The development of a novel urea sensor using polypyrrole. *Electrochim Acta* 145:19–26
22. Naoi K, Lien M, Smyrl WH (1991) Quartz crystal microbalance study: ionic motion across conducting polymers. *J Electrochem Soc* 138(2):440–445
23. Baker CK, Reynolds JR (1988) A quartz microbalance study of the electrosynthesis of polypyrrole. *J Electroanal Chem* 251(2):307–322
24. Suarez MF, Compton RG (1999) In situ atomic force microscopy study of polypyrrole synthesis and the volume changes induced by oxidation and reduction of the polymer. *J Electroanal Chem* 462(2): 211–221
25. Fakhry A, Cachet J, Debiemme-Chouvy C (2015) Mechanism of formation of templateless electrogenerated polypyrrole nanostructures. *Electrochim Acta* 179:297–303
26. Arjomandi J, Davood R, Fatemeh G (2016) Surface characterization and morphology of conducting polypyrrole thin films during polymer growth on ITO glass electrode. *J Phys Chem C* 120(32): 18055–18065
27. Suematsu S, Oura Y, Tsujimoto H, Kanno H, Naoi K (2000) Conducting polymer films of cross-linked structure and their QCM analysis. *Electrochim Acta* 45(22-23):3813–3821
28. Arca M, Mirkin MV, Bard AJ (1995) Polymer films on electrodes. 26. Study of ion transport and electron transfer at polypyrrole films by scanning electrochemical microscopy. *J Phys Chem* 99(14): 5040–5050
29. Tsai EW, Jang GW, Rajeshwar K (1987) Proton transport accompanies redox switching of polypyrrole: a spectroelectrochemical study. *J Chem Soc Chem Commun* 1776–1778
30. Torresi RM, de Torresi SIC, Matencio T, De Paoli M-A (1995) Ionic exchanges in dodecylbenzenesulfonate-doped polypyrrole. Part II: electrochemical quartz crystal microbalance study. *Synth Met* 72(3):283–287
31. Holzhauser P, Bouzek K (2006) Influence of counter-ions on the permeability of polypyrrole films to hydrogen. *J Appl Electrochem* 36:703–710